Alu insertion-mediated dsRNA structure formation with pre-existing *Alu* elements as a novel disease-causing mechanism

Emmanuelle Masson[1,2], Sandrine Maestri[1,2], Valérie Bordeau[3], David N. Cooper[4], Claude Férec,[1] Jian-Min Chen[1,*]

[1]Univ Brest, Inserm, EFS, UMR 1078, GGB, F-29200 Brest, France.
[2]CHRU Brest, Brest, France.
[3]Inserm U1230 BRM (Bacterial RNAs and Medicine), Université de Rennes, Rennes, France.
[4]Institute of Medical Genetics, School of Medicine, Cardiff University, Cardiff, United Kingdom

*Correspondence:
Jian-Min Chen, Univ Brest, Inserm, EFS, UMR 1078, GGB, Faculté de Médecine, 22 avenue Camille Desmoulins, F-29238 BREST Cedex 3, France.
Email: jian-min.chen@univ-brest.fr

Abstract

We previously identified a homozygous *Alu* insertion variant (*Alu*_Ins) in the 3'-UTR of the *SPINK1* gene as the cause of a novel pediatric disease. Although we established that *Alu*_Ins leads to the complete loss of *SPINK1* mRNA expression, the precise mechanisms remained elusive. Here we aimed to elucidate these mechanisms through a hypothesis-driven approach. Initially, we speculated that *Alu*_Ins could independently disrupt mRNA 3' end formation and/or affect other post-transcriptional processes such as nuclear export and translation, due to its particular location. However, the presence of *Alu*_Ins in the 3'-UTR resulted in only an ~50% reduction in luciferase reporter activity compared to the wild-type, suggesting the involvement of additional mechanisms. Using RepeatMasker, we identified two *Alu* elements within *SPINK1*'s third intron, both of which resided in an orientation opposite to that of *Alu*_Ins. Through RNAfold predictions and full-length gene expression assays designed to examine orientation-dependent interactions between *Alu* repeats, we present evidence linking the detrimental effect of *Alu*_Ins to extensive double-stranded RNA structures formed between *Alu*_Ins and pre-existing intronic *Alu* sequences. Our results reveal a novel pathogenetic mechanism involving an *Alu* insertion, highlighting the importance of considering interactions between new and pre-existing *Alu* elements in inverted orientations within disease-associated genes.

Keywords: aberrant splicing; double-stranded RNA (dsRNA) structure; full-length gene expression assay (FLGEA); inverted *Alu* elements; RNA secondary structure; *SPINK1* gene; 3'-UTR reporter assay

1. Introduction

Alu elements are short DNA sequences approximately 300 nucleotides in length, representing one of the most abundant types of mobile genetic element within primate genomes. They exceed one million copies in the human genome, constituting nearly 11% of the total genomic content [1]. *Alu* elements are continually amplified in the human genome through long interspersed element-1 (LINE-1 or L1)-mediated retrotransposition [2, 3], a mechanism also linked to various human genetic disorders (for reviews, see [2, 4-6]). Historically, disease-causing *Alu* insertions have invariably been identified within the coding or proximal intronic regions of affected genes, largely due to detection bias [7]. However, a new finding emerged in 2017 when a full-length *Alu* insertion, henceforth termed *SPINK1 Alu*_Ins, was identified for the first time outside of these conventional gene regions — it was found in the 3'-untranslated region (3'-UTR) of the *SPINK1* gene (MIM: 167790) in a patient presenting with severe infantile isolated exocrine pancreatic insufficiency, a novel pediatric disease [8]. This novel finding would not have been possible without the inclusion of the gene's 3'-UTR in the mutational screen. Additionally, the *Alu*_Ins variant might easily have been overlooked had it not been present in the homozygous state. More recent examples of *Alu* insertions identified outside the conventional coding or proximal intronic regions of disease genes include an *Alu*Jb element within the *SMN1/2* promoter region [9] and a 316 bp *Alu* insertion overlapping the *TMEM106B* 3'-UTR that is tightly linked with top GWAS variants associated with the increased risk of frontotemporal lobar dementia with TDP-43 inclusions (FTLD-TDP) [10].

The pathological implications of disease-causing *Alu* insertions within coding or proximal intronic regions are typically linked to their potential to disrupt coding sequences or to induce aberrant splicing, often leading to a lack of detailed experimental analysis. In our previous research, we explored the functional consequences of the *SPINK1 Alu*_Ins variant using a cell culture-based full-length gene expression assay (FLGEA) [8] (see also Figure 1). We found that, whereas the wild-type (WT) *SPINK1* expression vector produced normally spliced transcripts, the mutant (Mut) vector resulted in a complete absence of *SPINK1* mRNA expression in transfected HEK293T cells. This finding was supported by three distinct lines of evidence: First, reverse transcription-polymerase chain reaction (RT-PCR) analysis detected *SPINK1* transcripts in lymphocytes from a healthy control but failed to identify any *SPINK1* transcripts in lymphocytes from the *SPINK1 Alu*_Ins homozygote [8]. Second, a complete deletion of the entire *SPINK1* gene in the homozygous state, leading to complete loss of *SPINK1* expression, was found in another patient with severe infantile isolated exocrine pancreatic insufficiency [8]. Third, there were notable pathological similarities between the pancreatic conditions in these two patients and those in *Spink3*-deficient mice [11] (Note: *Spink3* is the murine equivalent of *SPINK1*). Importantly, the pancreatic conditions resulting from complete *SPINK1* functional loss were significantly more severe than those in *SPINK1* c.194+2T>C homozygotes with chronic pancreatitis, who retained about 10% of normal *SPINK1* function [12-14].

Despite these findings, the precise mechanisms underlying the complete loss of *SPINK1* mRNA expression due to *SPINK1 Alu*_Ins have remained elusive. In the present study, we aimed to elucidate these mechanisms through a hypothesis-driven approach.

72 ## 2. Materials and Methods

73 ### 2.1. Reference sequences

74 In line with our earlier studies [8, 13, 15], the pathophysiologically relevant, four-exon *SPINK1* gene [16, 17]
75 was employed as the reference. The corresponding mRNA reference sequence is NM_001379610.1. The
76 genomic sequence for *SPINK1* was sourced from the GRCh38/hg38 assembly, accessible at
77 https://genome.ucsc.edu/. Nucleotide numbering followed the coding DNA sequence guidelines established by
78 the Human Genome Variation Society [18].
79

80 ### 2.2. 3'-UTR luciferase reporter assay

81 *2.2.1. Construction of WT and Alu_Ins 3'-UTR reporter vectors*

82 The WT *SPINK1* gene's 3'-UTR spans 81 bp. To construct the WT 3'-UTR reporter vector, we amplified a 306-
83 bp fragment that includes the entire 3'-UTR (from c.*1 to c.*81) and the downstream 225-bp 3' flanking
84 sequence (from c.*82 to c.*306) of the *SPINK1* gene (see Supplementary Figure S1). This fragment was PCR-
85 amplified from genomic DNA obtained from a healthy individual using the forward primer 5'-
86 TCTAGAGAACCAAGGTTTTGAAATCCCA-3' (containing an *Xba*I restriction site, underlined) and the
87 reverse primer 5'-GGATCCGATCATCTGTGCTCTGCCAT-3' (containing a *BamH*I restriction site,
88 underlined). The corresponding fragment containing the *Alu*_Ins was amplified from genomic DNA obtained
89 from the homozygous patient. The resulting PCR products were firstly digested with *Xba*I and *BamH*I and then
90 cloned into the *XbaI*/*BamH*I sites of the pGL3 Control Vector (Promega, Charbonnieres, France), yielding the
91 pGL3-WT and pGL3-*Alu SPINK1* 3'-UTR reporter gene constructs, respectively. In each construct, the insert
92 was placed immediately after the translational termination codon of the luciferase reporter gene. The accuracy of
93 both inserts was confirmed through sequencing using the BigDye™ Terminator v1.1 Cycle Sequencing Kit
94 (ThermoFisher Scientific, Illkirch, France).
95

96 *2.2.2. Cell culture, transfection and luciferase reporter gene assay*

97 Human embryonic kidney (HEK293T) and human pancreatic adenocarcinoma (COLO-357) cell lines were
98 maintained in DMEM nutrient mixture supplemented with 10% fetal calf serum. Transfections were carried out
99 as previously described [19] using 3.8 µg pGL3-WT or pGL3-*Alu SPINK1* 3'-UTR luciferase reporter vector
100 plus 0.2 µg control pRL-CMV vector. At 48 h after transfection, luciferase activity was measured as previously
101 described [20].
102

103 ### 2.3. Identification of pre-existing *Alu* elements in the *SPINK1* locus using RepeatMasker

104 The search for *Alu* elements in the *SPINK1* locus was conducted using RepeatMasker
105 (http://www.repeatmasker.org/). Two *Alu* elements, identified in intron 3 of the gene, were designated *Alu*1 and
106 *Alu*2 respectively, as illustrated in Supplementary Figure S1 (see also Figure 1).
107

108 ### 2.4. Construction of five additional expression vectors for FLGEA

109 In our earlier research [8], we engineered expression vectors for both the full-length WT and the mutant (Mut)
110 *SPINK1* sequences, the latter containing the *Alu*_Ins variant, for the FLGEA assay (Figure 1). In this study, we
111 expanded our toolkit by developing five additional expression vectors tailored for the FLGEA assay. These new

vectors are designated as WT_del*Alu*1, Mut_del*Alu*1, WT_del*Alu*2, Mut_del*Alu*2, and Inv*Alu*_Ins, with 'Inv*Alu*_Ins' specifically referring to an inversion of the *Alu*_Ins sequence (Figure 1).

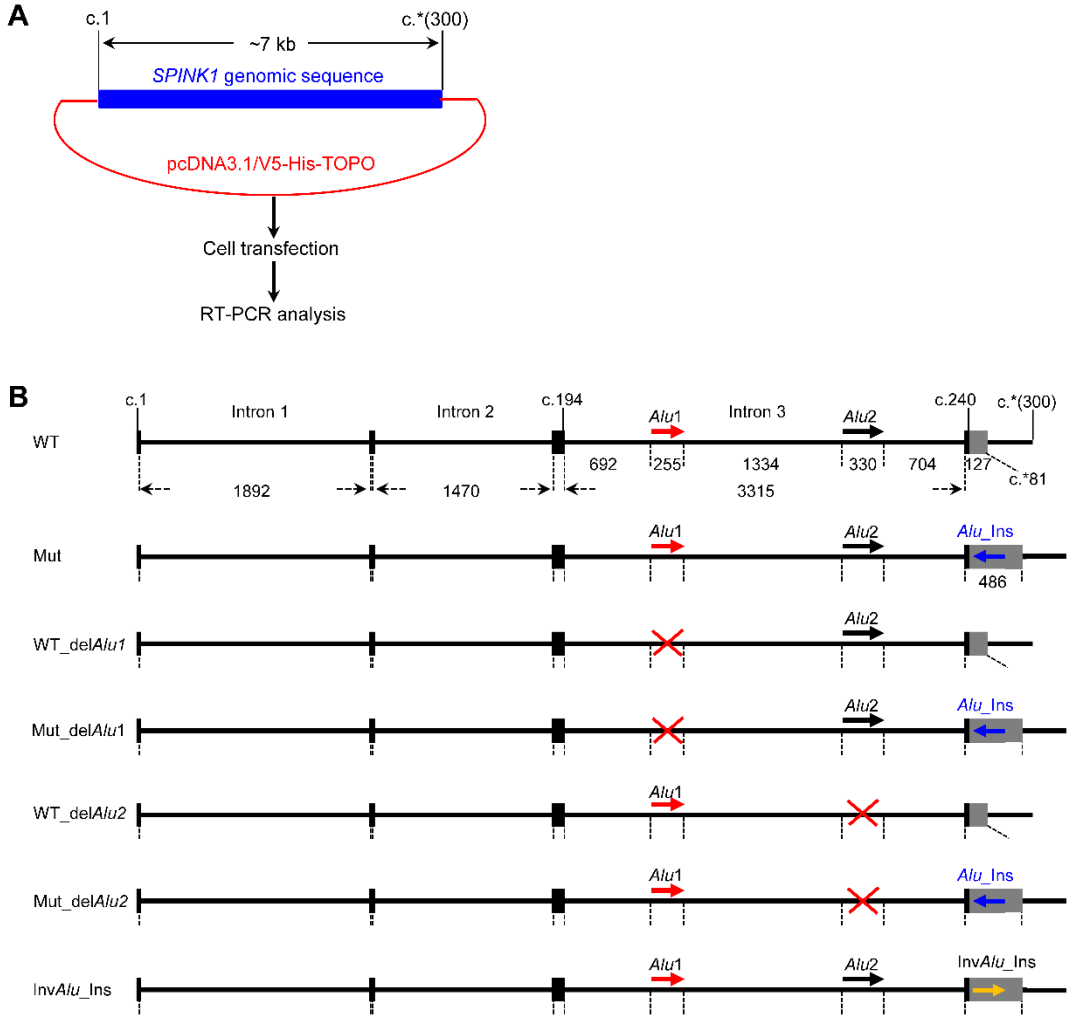

Figure 1. Illustration of the FLGEA assay and the seven expression vectors used in the current study. (**A**) Schematic representation of the expression vectors and the experimental procedures of the FLGEA assay. Each expression vector was constructed using the pcDNA3.1/V5-His TOPO vector as a backbone. The *SPINK1* sequences inserted in these vectors span from c.1 (the A of the ATG start codon) to c.*(300) (300 bases beyond the TGA stop codon), based on the WT *SPINK1* genomic sequence. For further sequence information, see Supplementary Figure S1. (**B**) Detailed depiction of the WT and Mut *SPINK1* sequences and the five novel artificial sequences developed for the FLGEA vectors in this study. The *SPINK1* genomic sequence is shown to scale, with coding regions indicated by black bars and the 3'-UTR as a grey box. The lengths (in bp) of the three introns and the two *Alu* elements (named *Alu*1 and *Alu*2) in intron 3 are specified. Positions c.194, c.240, and c.*81 correspond to the final nucleotide positions of exon 3, the translation termination codon, and the 3'-UTR, respectively. Horizontal solid arrows show the orientations of the pre-existing *Alu* elements in intron 3, the disease-associated *Alu* insertion (*Alu*_Ins), and the artificially inverted version of *Alu*_Ins (Inv*Alu*_Ins), with rightward arrows denoting alignment with the *SPINK1* gene's sense strand and leftward arrows indicating the opposite orientation. Artificial deletions of *Alu*1 or *Alu*2 in WT and Mut contexts are highlighted with red crosses. *Abbreviations:* FLGEA, full-length gene expression assay; Mut, mutant; RT-PCR, reverse transcription-polymerase chain reaction; WT, wild-type; 3'-UTR, 3'-untranslated region.

133 *2.4.1. Construction of the WT_delAlu1 and Mut_delAlu1 vectors*

134 To create *Alu*1 deletions within WT and Mut *SPINK1* contexts, we used genomic DNA from a healthy control
135 and the patient homozygous for *SPINK1 Alu*_Ins, respectively. Two specific DNA fragments were amplified
136 (color-coded primer pairs shown in Supplementary Figure S2A). For each fragment, a PCR reaction was
137 performed with 50 ng DNA in a 50 µL reaction mixture containing 2.5 U TaKaRa La Taq™ DNA polymerase,
138 400 µM TakaRa dNTP Mix, and 0.4 µM each of the corresponding primer pair. The PCR program comprised an
139 initial denaturation at 94°C for 1 min, 35 cycles of denaturation at 94°C for 20 s, annealing at 56°C for 20 s and
140 extension at 72°C for 5 min, and a final extension step at 72°C for 10 min. After *Kpn*I restriction enzyme
141 digestion, the two fragments from each DNA source were ligated, then further amplified with primers P1_F and
142 reverse primer P1_R (Supplementary Figure S2A). The PCR was performed using the GoTaq® Long PCR
143 MasterMix (Promega, Charbonnieres, France) according to the manufacturer's protocol. The PCR program had
144 an initial denaturation at 94°C for 2 min, 35 cycles of denaturation at 94°C for 20 s, annealing at 58°C for 20 s
145 and extension at 65°C for 6 min, and a final extension step at 72°C for 10 min. The final PCR products,
146 WT_del*Alu*1 and Mut_del*Alu*1, were separately cloned into the pcDNA3.1/V5-His TOPO vector according to
147 the manufacturer's instructions.
148

149 *2.4.2. Construction of the WT_delAlu2 and Mut_delAlu2 vectors*

150 These vectors were constructed following the same methodology as applied to WT_del*Alu*1 and Mut_del*Alu*1,
151 but they employed distinct sets of primer pairs, as detailed in Supplementary Figure 2B. Furthermore, the PCR
152 amplification extension times were adjusted according to the lengths of the fragments: 6 min for the longer
153 fragment (amplified using P1_F and *Alu*2_*KpnI*_R primers) and 1 min for the shorter fragment (amplified using
154 *Alu2_KpnI*_F and P1_R primers).
155

156 *2.4.3. Construction of the InvAlu_Ins vector*

157 To develop the Inv*Alu*_Ins vector, intended for reversing the orientation of the *Alu*_Ins sequence within the 3'-
158 UTR of the *SPINK1* gene, we first eliminated a pre-existing *Nco*I restriction site found in the third intron of the
159 Mut vector. This alteration was performed using the QuickChange II XL Site-Directed Mutagenesis Kit with the
160 application of specific primers: forward 5'-
161 TGGCCAACATGGTGAAACCCCGTGGTGGCGGGCGCCTATAATAC-3' and reverse 5'-
162 GTATTATAGGCGCCCGCCACCACGGGGTTTCACCATGTTGGCCA-3'. After modification, three separate
163 fragments were PCR-amplified from the modified plasmid template. Each PCR reaction used 1 ng of the altered
164 plasmid in a 50 µL reaction mix, which included 2.5U TaKaRa La Taq™ DNA polymerase, 400 µM TaKaRa
165 dNTP Mix, and 0.4 µM of each primer in the corresponding pair (Supplementary Figure 2C). The PCR
166 conditions were set as follows: initial denaturation at 94°C for 1 min, followed by 35 cycles of 20 s at 94°C for
167 denaturation, 20 s at 56°C for annealing, and extension at 72°C for 7 min for fragment A and 1 min for
168 fragments B and C. This was concluded with a final extension at 72°C for 10 min. The three resulting fragments
169 were individually digested with *Kpn*I and/or *Nco*I restriction enzymes and subsequently ligated together. The
170 steps following this ligation were conducted in the same manner as outlined earlier for additional vector
171 constructs.

172 Primer sequences related to the construction of the five new expression vectors are provided in
173 Supplementary Figure 2D. The exon/intron boundaries and ligation junctions within the resulting vector
174 constructs were verified through sequencing.
175
176 **2.5. FLGEA**
177 *2.5.1. Cell culture, transfection and reverse transcription (RT)*
178 HEK293T cells were maintained as described in section 2.2.2. For transfections, 1 µg of the corresponding
179 expression plasmid was used per well in a 6-well plate. Four hours prior to RNA extraction, the cells underwent
180 treatment with 50 µg/ml cycloheximide as previously described [21]. Total RNA was extracted from the cells 24
181 h post-transfection using TRIzol RNA Isolation Reagents (ThermoFisher Scientific). The purity and
182 concentration of the RNA were assessed based on the optical density (OD) measurements at 260 nm and 280 nm.
183 For RT, 4 µg RNA was first treated with DNase I (ThermoFisher Scientific, Illkirch, France) to eliminate
184 any contaminating DNA. The RT reaction was prepared in a 20 µL volume, including 1 µg DNase I-treated
185 RNA, 10 U RNAse inhibitor (Promega, Charbonnieres, France), 250 ng Oligo(dT) (Qiagen, Courtaboeuf,
186 France), 4 µl 5× First Strand Buffer, 500 µM dNTPs, 5 mM dithiothreitol, and 200 U SuperScript® II Reverse
187 Transcriptase (ThermoFisher Scientific, Illkirch, France). The reaction mixture was incubated at 42°C for 50 min
188 and then deactivated by heating at 70°C for 15 min. After RT, the cDNA was treated with 2 U RNase H
189 (ThermoFisher Scientific, Illkirch, France) to remove any remaining RNA, at 37°C for 20 min.
190
191 *2.5.2. RT-PCR*
192 RT-PCR was conducted using the forward primer 5'-GAGTCTATCTGGTAACACTGGAGCT-3' and reverse
193 primer 5'-CAGTCAGGCCTCGCGGTG-3', employing the GoTaq® Long PCR MasterMix in accordance with
194 the manufacturer's instructions. The PCR cycle commenced with an initial denaturation at 94°C for 2 min, then
195 proceeded through 40 cycles of 20 s at 94°C for denaturation, 20 s at 58°C for annealing, and 4 min at 65°C for
196 extension. This was concluded with a final extension phase at 72°C for 5 m. The PCR products were
197 subsequently analyzed by electrophoresis on a 1% agarose gel.
198
199 *2.5.3. Sequencing of the RT-PCR products*
200 The RT-PCR products derived from the WT, WT_del*Alu*1, WT_del*Alu*2, and Inv*Alu*_Ins expression vectors
201 were purified using the Illustra™ ExoProStar™ (GE Healthcare, Orsay, France). Subsequently, they were
202 directly sequenced utilizing the BigDye™ Terminator v1.1 Cycle Sequencing Kit, employing the forward primer
203 5'-GAGTCTATCTGGTAACACTGGAGCT-3' and the reverse primer 5'-CAGTCAGGCCTCGCGGTG-3'.
204 RT-PCR products from the Mut, Mut_del*Alu*1, and Mut_del*Alu*2 expression vectors were individually
205 cloned into the pcDNA3.1/V5-His TOPO vector, following the manufacturer's guidelines. Transformation
206 employed XL10-Gold Ultracompetent Cells (Stratagene, La Jolla, CA). The transformed cells were plated on LB
207 agar containing 50 mg/mL ampicillin and incubated at 37ºC overnight. Approximately 30 colonies from each
208 transformation were selected for PCR amplification using the GoTaq® Long PCR MasterMix, in line with the
209 manufacturer's instructions. The PCR utilized forward primer 5'-GGAGACCCAAGCTGGCTAGT-3' and
210 reverse primer 5'-AGACCGAGGAGAGGGTTAGG-3', both situated within the vector sequence. The
211 amplification protocol started with an initial denaturation at 94°C for 2 min, followed by 35 cycles of 20 s at

212 94°C for denaturation, 20 s at 58°C for annealing, and extension at 65°C for 1 min (for Mut and Mut_del*Alu*2) or
213 4 min (for Mut_del*Alu*1), culminating in a final extension at 72°C for 5 min. PCR products were assessed via
214 electrophoresis on a 1% agarose gel, then purified using Illustra™ ExoProStar™, and sequenced employing the
215 BigDye™ Terminator v1.1 Cycle Sequencing Kit. Sequencing utilized primers 5'-
216 GGAGACCCAAGCTGGCTAGT-3' (forward), 5'-TGAAAATCGGTGAGTACA-3' (forward), 5'-
217 GAAAACATCATGAGCATG-3' (forward), and 5'-AGACCGAGGAGAGGGTTAGG-3' (reverse). For the
218 larger band (>2 kb) derived from Mut_del*Alu1*, additional sequencing employed three forward primers: 5'-
219 CTGAGATTGACTTGAT-3', 5'-TCTGAAACCTCCGAGT-3', and 5'-CTAACTTAAATGTGGCT-3'.
220 Bands whose identities remained uncertain following the initial sequencing were excised from the agarose
221 gel and purified using the MinElute Gel Extraction Kit (Qiagen, Courtaboeuf, France). These purified fragments
222 were then sequenced using the BigDye™ Terminator v1.1 Cycle Sequencing Kit. The sequencing employed
223 forward primer 5'-GAGTCTATCTGGTAACACTGGAGCT-3' and reverse primer 5'-
224 CAGTCAGGCCTCGCGGTG-3.
225
226 *2.5.4. Quantification of RT-PCR bands using ImageJ*
227 The intensities of the RT-PCR bands of interest were quantified with ImageJ.JS software, accessible at
228 https://ij.imjoy.io/.
229
230 *2.5.5. Additional RT-PCR analysis*
231 For the purpose of amplifying potential transcripts that retain intron 3 but correctly exclude introns 1 and 2, as
232 detected in the FLGEA assay using the Mut vector, we employed various primer combinations for additional
233 PCR analyses on the above prepared cDNA. The three utilized forward primers were: one located in the
234 promoter region of the pcDNA3.1 vector (5'-TGGTGGAATTGCCCTTATGA-3'), one spanning the junction
235 between *SPINK1* exons 1 and 2 (5'-GAGTCTATCTGGTAACACTGGAGCT-3'), and one spanning the
236 junction between *SPINK1* exons 2 and 3 (5'-TGGGAAGAGAGGCCAAATGT-3'). The three reverse primers
237 were all positioned within intron 3, specifically between the *Alu*1 and *Alu*2 regions (5'-
238 CCAAGAAGAAGGTTTGCATTAC-3', 5'-CTTGGAAATTTCCCAAGTCTC-3', and 5'-
239 GCATAAACATAGAACATTTCCATC-3').
240
241 **2.6. Prediction of RNA secondary structures using RNAfold**
242 RNA secondary structures were predicted using the RNAfold tool, which is part of the Vienna RNA Websuite
243 (http://rna.tbi.univie.ac.at/), under default parameters [22]. The analysis covered sequences from the start of exon
244 3 to the end of the 3'-UTR (i.e., c.*81 in the context of the WT *SPINK1* gene). For the exact sequences of the
245 five alleles (WT, Mut, Inv*Alu*_Ins, Mut-del*Alu*1, and Mut_del*Alu*2) used in the secondary structure prediction,
246 see Supplementary Figures S3-S7.
247
248 ## 3. Results
249 **3.1. Evaluation of the hypothesis: independent impact of *SPINK1 Alu*_Ins on gene expression**
250 The 3'-UTRs of human genes serve critical roles in regulating mRNA 3' end formation, stability, degradation,
251 nuclear export, subcellular localization, and translation processes [23-26]. Building on this understanding, we

252 initially hypothesized that the *SPINK1 Alu*_Ins variant might independently influence one or more of these
253 regulatory functions due to its particular insertion location. This could potentially explain the previously
254 observed complete absence of *SPINK1* mRNA expression [8]. To investigate this hypothesis, we conducted a 3'-
255 UTR luciferase reporter assay to assess the overall impact of the *SPINK1 Alu*_Ins variant on the aforementioned
256 regulatory processes. The 3'-UTR vector containing the *Alu*_Ins variant resulted in a significant decrease in
257 luciferase activity, demonstrating approximately a 50% reduction compared to the wild-type control in both
258 HEK293T and COLO-357 cell lines (Figure 2). However, this reduction alone does not fully account for the total
259 absence of *SPINK1* expression observed previously [8], suggesting the presence of additional mechanisms that
260 warrant further exploration.
261

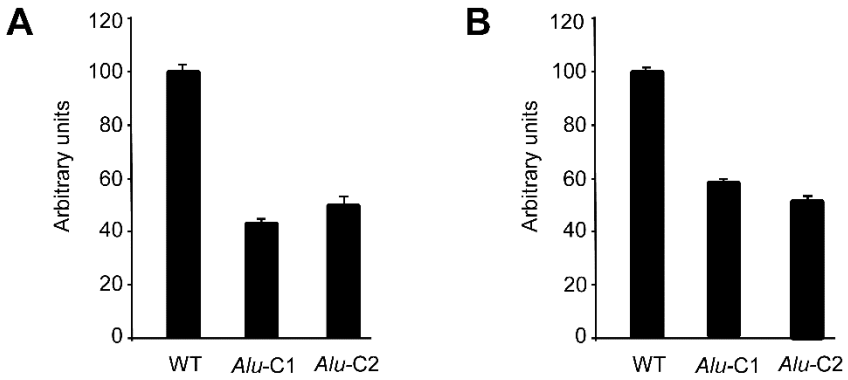

262
263
264 **Figure 2**. 3'-UTR luciferase reporter assay outcomes. Transfections were performed in HEK293T (**A**) and COLO-
265 357 (**B**) cells. "WT" refers to the wild-type *SPINK1* 3'-UTR luciferase reporter vector, whereas "*Alu*-C1" and "*Alu*-
266 C2" denote two distinct clones of the mutated *SPINK1* 3'-UTR luciferase reporter vector. Data are shown as the
267 average ± standard deviation from three separate experiments, each carried out in triplicate.
268

269 **3.2. Formulation of a new hypothesis: impact of *Alu*_Ins on long double-stranded RNA (dsRNA) structure**
270 **formation with pre-existing *Alu* elements in the *SPINK1* gene**

271 A limitation of the 3'-UTR reporter assay lies in its inherent inability to assess the potential impact of the studied
272 variant on splicing. Splicing, a complex process preceding mRNA 3' end formation and other post-transcriptional
273 events, is fundamental to gene expression [27-29]. The gene's primary sequence, encoding regulatory elements
274 and secondary structures, establishes the groundwork for mRNA splicing outcomes.

275 RNA secondary structures, dependent upon the primary sequence, significantly influence alternative splicing
276 [30, 31]. Alterations in pre-mRNA secondary structure are linked to the pathological effects of numerous
277 disease-associated variants [32, 33]. The abundance of *Alu* elements in the human genome, with their sequence
278 similarities, makes inverted *Alu* repeats a major source for dsRNA structure formation. Notably, there are
279 228,607 inverted *Alu* pairs within 1 kb of each other in genes from the NCBI Reference Sequence (RefSeq)
280 database [34]. Genome-wide analyses reveal that dsRNA structures frequently form between inverted *Alu*
281 elements located within a distance of <800 bp apart, although they can also occur over distances of several
282 thousand bp [35]. Recent research utilizing the J2 antibody has directly mapped dsRNA structures from inverted
283 *Alu* elements in 3'-UTRs [36]. Additionally, artificial *Alu* sequences inserted in opposite orientations within an
284 intron of a three-exon-minigene formed base pairings, thereby altering the splicing pattern of the downstream
285 exon [37]. Lastly, the emergence of circular RNAs (circRNAs), a class of RNAs identified recently [38], is

286 thought to result from back-splicing mechanisms [39]. Such mechanisms often depend on secondary structures in
287 pre-mRNAs, especially those formed by inverted *Alu* elements [40-42].
288 Based on these findings, we hypothesize that the *SPINK1 Alu*_Ins variant could induce the formation of long
289 dsRNA structures with pre-existing *Alu* elements in the *SPINK1* gene, potentially impacting splicing, one of the
290 initial stages of mRNA formation.
291
292 **3.3. Discovery of two oppositely oriented *Alu* elements in intron 3 of *SPINK1* gene relative to *Alu*_Ins**
293 To establish the plausibility of our new hypothesis, two specific conditions would need to be met: Firstly, there
294 must be pre-existing *Alu* elements within the *SPINK1* gene locus. Secondly, these pre-existing elements must be
295 oriented inversely compared to the *Alu*_Ins variant. Using the RepeatMasker tool
296 (http://www.repeatmasker.org/), we identified two such pre-existing *Alu* elements within intron 3 of the *SPINK1*
297 gene, designated as *Alu*1 and *Alu*2, respectively. As illustrated in Supplementary Figure S1 and Figure 1, both
298 *Alu*1 and *Alu*2 exhibit the opposite orientation to the *Alu*_Ins variant, thereby supporting our hypothesis.
299 Furthermore, we observed that the pre-existing *Alu*2 element and the pathogenic *Alu*_Ins variant are separated by
300 <800 bp. This close proximity is noteworthy, as inverted *Alu* repeats within such short distances often lead to the
301 formation of dsRNA structures [35], which aligns with our investigative premise.
302
303 **3.4. Prediction of long dsRNA stem formation between *Alu*_Ins and *Alu*2 using RNAfold**
304 We employed RNAfold (http://rna.tbi.univie.ac.at/) [22], with default settings, to assess the potential secondary
305 structures of the pre-mRNA of the Mut (*Alu*_Ins) allele, with the WT allele used for comparison. Our analysis
306 encompassed sequences from the beginning of exon 3 to the end of the 3'-UTR (for the exact sequences, see
307 Supplementary Figures S3 and S4). The minimum free energy (MFE) structures obtained, depicted in Figure 3,
308 reveal the presence of an extensive dsRNA stem, covering 259 bp in *Alu*2 and 270 bp in *Alu*_Ins (refer to
309 Supplementary Figure S4 for further details).
310
311 **3.5. Restoration of *SPINK1* mRNA expression by disrupting long dsRNA stem formation**
312 Given the established role of (i) inverted *Alu* repeats in forming long dsRNA stems and (ii) RNA secondary
313 structure on gene splicing and expression, our findings would draw a direct link between the intricate dsRNA
314 structure formed through the interaction of *Alu*2 and *Alu*_Ins and the absence of *SPINK1* expression. To delve
315 deeper, we developed five new vectors for the FLGEA assay, notably introducing an inverted version of *Alu*_Ins,
316 termed Inv*Alu*_Ins (see Figure 1). This modification aimed to prevent the formation of detrimental dsRNA
317 structures by aligning all three *Alu* elements in the same direction, potentially restoring gene expression.
318 RNAfold analysis confirmed that Inv*Alu*_Ins does not form extensive dsRNA stems (Figure 3). Despite the
319 nearly identical lengths of the Mut and Inv*Alu*_Ins sequences (3908 bp versus 3909 bp, respectively), noticeable
320 differences were observed in their predicted MFE values: Mut exhibited -1265.90 kcal/mol, whereas Inv*Alu*_Ins
321 showed -1033.00 kcal/mol. This discrepancy apparently arises from the extensive dsRNA stem within Mut.
322 Furthermore, the significant difference in MFE between Mut and WT (-1265.90 kcal/mol vs. -890.80 kcal/mol)
323 underscores the cumulative effects of increased sequence length and dsRNA structure in Mut. Generally, a more
324 negative MFE indicates a stronger and more stable structure, whereas a less negative value suggests a weaker,
325 less compact structure.

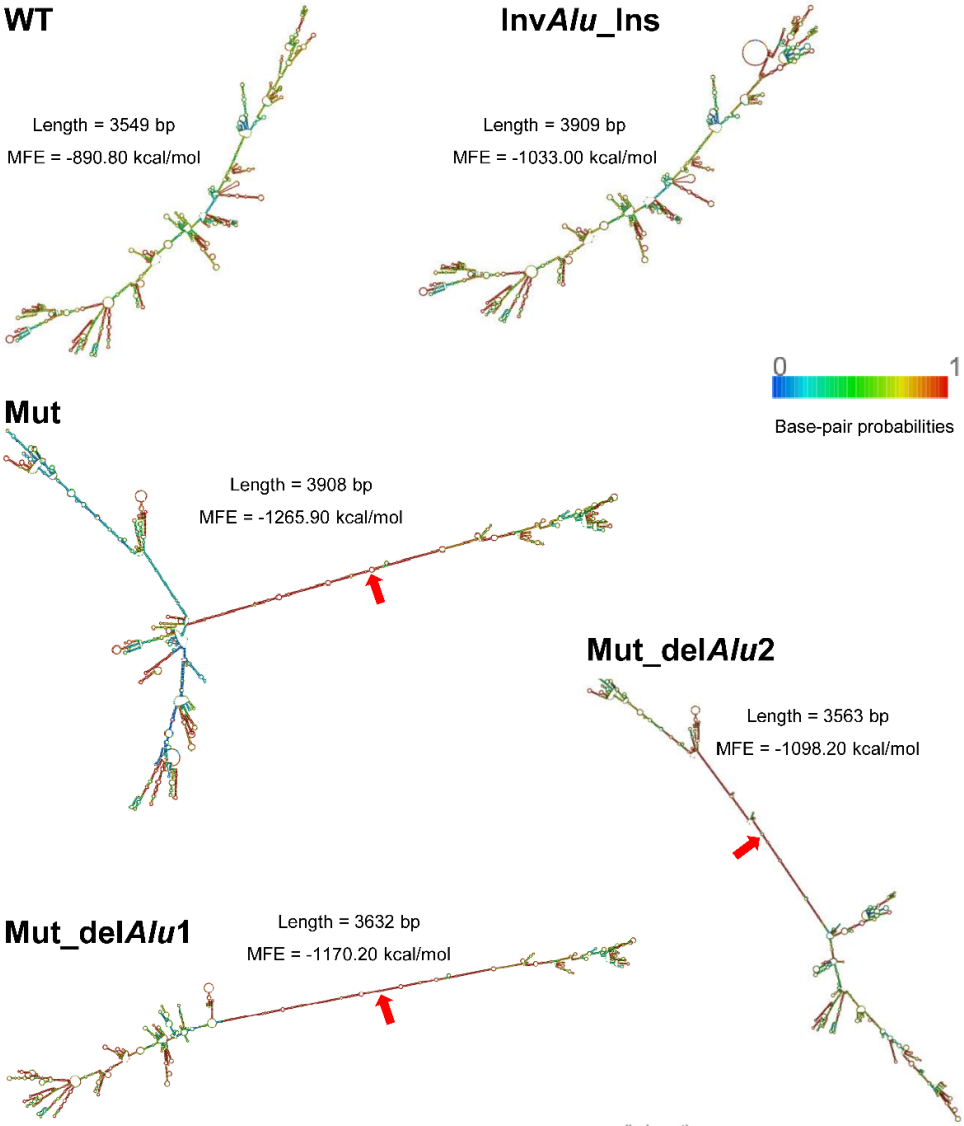

Figure 3. Minimum free energy (MFE) RNA secondary structures predicted by RNAfold for various *SPINK1* alleles. Refer to Figure 1 for a schematic representation of the different alleles. For each allele, the sequence used for prediction spans from the start of exon 3 to the end of the 3'-UTR of the *SPINK1* gene, with the corresponding length and MFE value specified within the Figure. Red arrows indicate the extended double-stranded RNA (dsRNA) stems formed between inverted *Alu* elements. The exact sequences employed in predicting RNA secondary structures are provided in Supplementary Figures S3-S7.

The Inv*Alu*_Ins vector, along with the other four newly designed vectors, was employed in the FLGEA assay together with the WT and Mut vectors. These assays were conducted under cycloheximide treatment, with the aim of revealing transcripts potentially masked by nonsense-mediated mRNA decay (NMD) in our previous research [8]. To begin, we shall discuss the results from the Inv*Alu*_Ins vector, comparing them to those from the WT and Mut vectors.

The reorientation of *Alu*_Ins within the Inv*Alu*_Ins vector effectively restored correctly spliced *SPINK1* transcripts. This was demonstrated by the detection of a distinct, clear band (identified as band G in Figure 4) in the RT-PCR analysis of HEK293T cells transfected with the Inv*Alu*_Ins vector; sequencing confirmed this band as representing correctly spliced transcripts containing the Ivs*Alu*_Ins sequence in the 3'-UTR. By contrast, cells

transfected with the Mut vector displayed two distinct aberrant bands (labeled as bands A and B in Figure 4) and one faint band (referred to as band C in Figure 4). Sequencing identified the faint band C as correctly spliced transcripts that include *Alu*_Ins within the 3'-UTR.

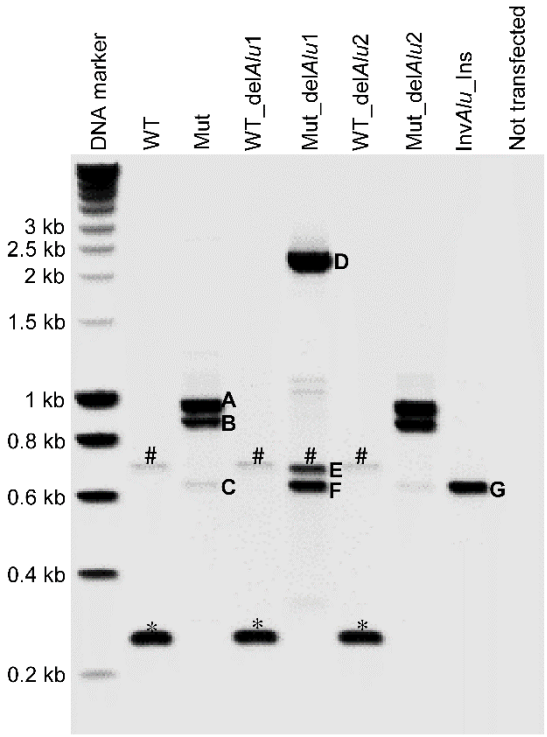

Figure 4. Outcomes of RT-PCR analysis on HEK293T cells transfected with various expression vectors. See Figure 1 for the schematic representation of the seven constructs. Bands marked with an asterisk indicate normally spliced wild-type *SPINK1* transcripts, while those with a hash represent non-specific amplifications. Bands C and F correspond to normally spliced transcripts containing *Alu*_Ins within the 3'-UTR, while band G corresponds to normally spliced transcripts that include Inv*Alu*_Ins within the 3'-UTR. Bands A, B, and D feature transcripts indicative of RNA template switching, facilitated by inverted *Alu* repeats. The characteristics of the three bands observed in Mut_del*Alu*2 closely mirror those in Mut.

The presence of the faintly spliced C band, alongside the two more pronounced aberrant bands (bands A and B), in cells transfected with the Mut vector in this study could be attributed to the effects of cycloheximide or differences in experimental conditions compared to our earlier study [8]. Nonetheless, the level of normally spliced transcripts in the Mut vector is notably low compared to either the co-amplified aberrant transcripts (bands A and B) observed in the Mut vector, the normally spliced transcripts detected with the WT vector (the leftmost band marked with an asterisk), or the normally spliced transcripts detected with the Inv*Alu*_Ins vector (band G). For example, the intensity of the faint C band from the Mut vector was measured to be only 4% of that of the G band from Inv*Alu*_Ins, as quantified using ImageJ.JS (https://ij.imjoy.io/). This substantially reduced level of normally spliced transcripts is consistent with the previously observed absence of *SPINK1* expression [8].

3.6. Further exploration of the impact of dsRNA formation on *SPINK1* expression by deletion of pre-existing *Alu*1 or *Alu*2 in the Mut context

370 The additional four vectors, designed with deletions of *Alu*1 or *Alu*2 elements within both the WT and Mut
371 contexts, were utilized to further examine the effect of dsRNA formation on *SPINK1* expression. The results
372 from the FLGEA assay, outlined in Figure 4, demonstrate that the WT context deletions, specifically
373 WT_del*Alu*1 and WT_del*Alu*2, produced normally spliced WT transcripts, akin to those from the original WT
374 vector, as evidenced by the second and third bands marked with asterisks. These observations imply that the
375 deletions did not inadvertently create new splicing signals and confirm that neither *Alu*1 or *Alu*2 would have
376 played a significant role in regulating *SPINK1* splicing within their original WT sequence context.
377 Using RNAfold, both the Mut_del*Alu*1 and Mut_del*Alu*2 alleles were predicted to develop significant
378 dsRNA stem structures due to inverted *Alu* repeats, as illustrated in Figure 3. Specifically, interactions were
379 noted between *Alu*2 and *Alu*_Ins in Mut_del*Alu*1 and between *Alu*1 and *Alu*_Ins in Mut_del*Alu*2 (see
380 Supplementary Figures S6 and S7 for details). Consequently, despite being shorter than the Inv*Alu*_Ins sequence,
381 which does not form extensive dsRNA structures, both Mut_del*Alu*1 and Mut_del*Alu*2 exhibited more negative
382 MFE values compared to InvAlu_Ins (Figure 3).
383 Consistent with the predicted long dsRNA stem structures, we observed a marked decrease in normally
384 spliced *SPINK1* transcripts with Mut_del*Alu*1 and almost total suppression with Mut_del*Alu*2 in the FLGEA
385 assay. Specifically, after length adjustment, normally spliced *SPINK1* transcripts in Mut_del*Alu*1 (represented by
386 band F in Figure 4) constituted about 90% of the level seen with the aberrantly spliced band D, signifying that
387 under 45% of the total transcripts were normally spliced. By contrast, the RT-PCR results for Mut_del*Alu*2
388 closely matched those of the Mut allele. These results confirm the profound effect of dsRNA stem structures on
389 gene splicing.
390
391 **3.7. Aberrant RT-PCR bands harboring sequence features consistent with dsRNA formation**
392 To identify the origins of the bands from the FLGEA, colony PCR analysis was conducted on the overall RT-
393 PCR products for each vector, complemented by sequencing of excised bands when necessary. The results for
394 the Mut vector—including the number of sequenced colonies and the characteristics of the RT-PCR products
395 corresponding to bands A, B, and C—are shown in the left panel of Figure 5A. Sequences from over half (15 out
396 of 29) of the informative Mut-derived colonies were consistent with normally spliced transcripts, associated with
397 band C. The unusually high representation of band C, despite its faint appearance, is likely due to a cloning bias
398 favoring shorter inserts (via ligation efficiency) during the cloning of RT-PCR products into the pcDNA3.1/V5-
399 His TOPO vector.
400 From the remaining 14 informative Mut-derived colonies, five distinct products were identified. Three of
401 these (A1, A2, and A3) corresponded to band A, and the other two (B1 and B2) to band B, as depicted in Figure
402 5A. The structure of these transcripts included exon 1, exon 2, exon 3, followed by a portion of the 5' proximal
403 part of intron 3, and a truncated 3'-UTR sequence. This pattern indicates that while introns 1 and 2 were
404 correctly excised, intron 3 was partially retained, accompanied by significant internal deletions affecting both
405 intron 3 and the 3'-UTR sequences. Importantly, the deletion junctions featured short direct repeats: one located
406 within the *SPINK1 Alu*_Ins and another within the retained section of intron 3. These direct repeats within
407 *SPINK1 Alu*_Ins were concentrated within a specific 20-bp segment, in contrast to those in intron 3, which were
408 spread across a stretch less than 100-bp. This particular 20-bp segment within *SPINK1 Alu*_Ins is found near the

3' end of *Alu*_Ins, whereas the less than 100-bp segment in intron 3 encompasses the 5' end of *Alu*1, as illustrated in Figure 5B.

A

Colony PCR analysis of RT-PCR products from HEK293T cells transfected with the Mut construct

Number of colonies sequenced (n=31)	Nature of sequence	Band assignment
2	A1	A
3	A2	A
2	A3	A
1	B1	B
6	B2	B
15	Correctly spliced	C
2	Not readable	—

Colony PCR analysis of RT-PCR products from HEK293T cells transfected with the Mut-del*Alu*1 construct

Number of colonies sequenced (n=30)	Nature of sequence	Band assignment
2	D1	D
6	D2	D
12	Correctly spliced	F
10	Not readable	—

B

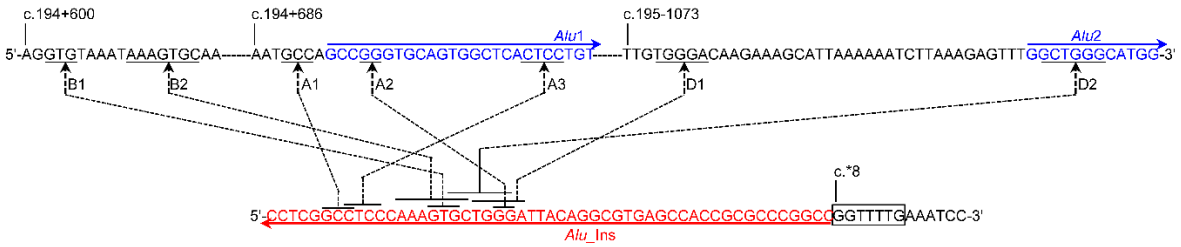

Figure 5. Results from colony PCR and sequencing analysis of FLGEA-derived RT-PCR bands. (**A**) Analysis of RT-PCR products from cells transfected with the Mut construct (left panel) or the Mut_del*Alu*1 construct (right panel). Refer to Figure 4 for the indicated bands. (**B**) Illustration of the presumed template switching events and their associated direct short repeats (indicated by underlines and overlines), responsible for the formation of aberrant transcripts (for more information, refer to the text). The boxed GGTTTG indicates the target site duplication. Nucleotide positions are designated according to the wild-type *SPINK1* sequence following the coding DNA sequence guidelines established by the Human Genome Variation Society [18]. *Abbreviations:* FLGEA, full-length gene expression assay; RT-PCR, reverse transcription-polymerase chain reaction.

The identified sequence characteristics hint at a possible reverse transcriptase template switching mechanism [43], presumably instigated by dsRNA structures forming between *Alu*1 and *SPINK1 Alu*_Ins in the mutant pre-mRNA sequences. These structures might initially impede the proper splicing of intron 3 during pre-mRNA splicing and subsequently foster template switching during the reverse transcription of mutant mRNAs harboring dsRNA, thereby culminating in the emergence of bands A and B, as elaborated in the left panel of Figure 6. However, our attempts to verify the hypothesized full-length transcripts—those retaining intron 3 while accurately excluding introns 1 and 2—using different primer combinations were unsuccessful.

Colony PCR and sequencing investigations revealed that the three bands emerging from the deletion of *Alu*2 in the mutant *SPINK1* context (Mut_del*Alu*2) bore a close resemblance to those identified with the Mut vector (Figure 4). This congruence is logical, as the anomalous bands A and B in the Mut vector were likely spawned from the interplay between *Alu*1 and *Alu*_Ins. In the Mut_del*Alu*2 construct, *Alu*1 persists as the singular pre-existing *Alu* element poised for interaction with *Alu*_Ins.

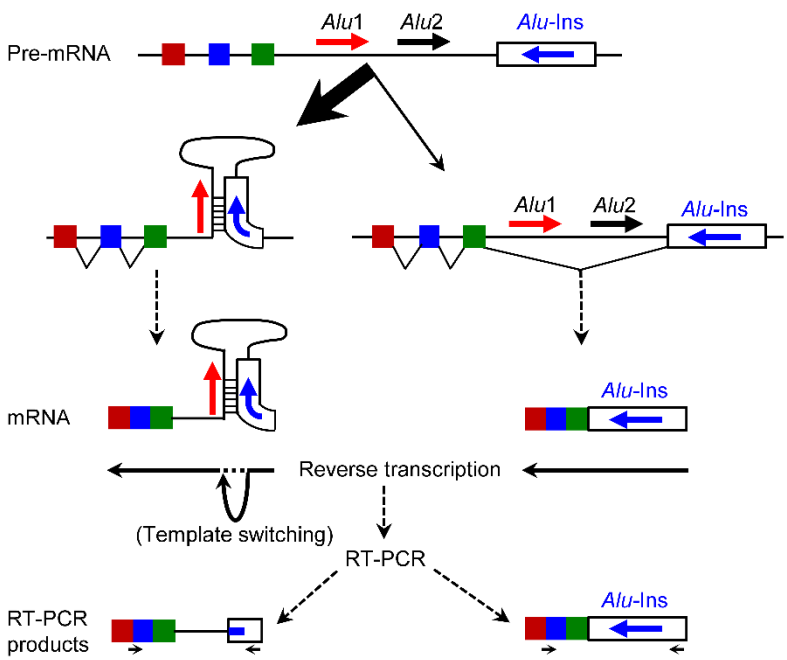

Figure 6. A schema to explain RT-PCR band formation in the FLGEA assay using the Mut vector. The components of the *SPINK1* genomic sequence are not to scale. The left panel demonstrates the production of the aberrant bands, while the right panel shows the creation of the faint band associated with normally spliced transcripts. In the bottom section, "RT-PCR products," the facing arrows depict the approximate locations of the primers used for RT-PCR analysis: the forward primer spans the junction between exons 1 and 2, and the reverse primer corresponds to nucleotides c.29_46 of the *SPINK1* gene's 3'-UTR. *Abbreviations:* FLGEA, full-length gene expression assay; RT-PCR, reverse transcription-polymerase chain reaction; 3'-UTR, 3'-untranslated region.

For the Mut_del*Alu*1 vector, band F (Figure 4) typifies normally spliced transcripts. Efforts to sequence the gel-purified band E product were unsuccessful, yielding no discernible sequence after multiple attempts. Band D was found to comprise two disparate entities, D1 and D2, as depicted in the right panel of Figure 5A. It is noteworthy that D1 and D2 transcripts exhibit parallel attributes to the Mut-derived bands A and B. They correctly splice through introns 1 and 2, diverging at intron 3, which is followed by the 3'-UTR and suffers from a substantial internal deletion. The deletion junctions also feature short direct repeats: one within the *SPINK1* *Alu*_Ins, located in the previously noted 20-bp segment, and the other within the sequence immediately upstream of the 5' end of *Alu*2 (Figure 5B). This outcome is logical, given that in the Mut_del*Alu*1 construct, *Alu*2 is the sole remaining pre-existing *Alu* element that can interact with *Alu*_Ins. Thus, the mechanism postulated for the creation of Mut-derived bands (Figure 6) might similarly explain the formation of bands from Mut_del*Alu*1, emphasizing the significant influence of dsRNA stem structures on the splicing process.

4. Discussion

In this study, our objective was to determine the mechanisms underlying the complete loss of *SPINK1* gene expression associated with the homozygous *Alu* insertion (*Alu*_Ins) in the gene's 3'-UTR [8]. Through a hypothesis-driven approach informed by current literature, we first identified pre-existing *Alu* elements within the third intron of the *SPINK1* gene, oriented in opposition to *Alu*_Ins. We then employed RNAfold predictions along with experimental data from a genomic context-preserving FLGEA assay, providing strong evidence that *Alu*_Ins's harmful effects arise from its formation of extensive dsRNA structures with these pre-existing *Alu*

462 sequences. Crucial evidence to the contrary came from the Inv*Alu*_Ins construct, an inverted version of the *Alu*
463 insertion that aligns all three *Alu* elements in the same direction, thereby inhibiting dsRNA formation. This setup
464 markedly contrasted with the Mut construct, which contains inverted *Alu* elements, sharply defining the role of
465 *Alu* orientation and dsRNA structures in affecting gene expression.
466 Our findings are further reinforced by additional assays conducted with the FLGEA assay, focusing on the
467 effects of deleting either the *Alu*1 or *Alu*2 elements. The outcomes of these deletion experiments were significant
468 for two reasons. Firstly, the continued presence of inverted *Alu* elements in both Mut_del*Alu*1 and Mut_del*Alu*2
469 meant that a suppressive effect on gene expression was both expected and observed in the FLGEA assay.
470 Secondly, and more intriguingly, the extent of suppression varied between the two. Contrary to initial
471 expectations, Mut_del*Alu*1, but not Mut_del*Alu*2, showed a reduction in repressive impact on gene expression.
472 This was surprising because *Alu*2 is physically closer to *Alu*_Ins than *Alu*1, and RNAfold predictions had
473 indicated a potential interaction between *Alu*2 and *Alu*_Ins (Figure 3). This finding from the FLGEA assay
474 implies that the *in vivo* effects of interactions between inverted *Alu* repeats on gene expression are complex,
475 influenced by a variety of factors such as their proximity, sequence similarity, and possibly others. It is
476 conceivable that, in a living organism, two *Alu* repeats positioned far apart and in opposite orientations could be
477 brought into close proximity by complex RNA structures. It is also worth noting that in the Mut context, there
478 were two pre-existing *Alu* elements, and RNAfold might have shown a preference for *Alu*2's interaction with
479 *Alu*_Ins over *Alu*1's interaction. In summary, this comparative approach not only corroborates our initial findings
480 but also deepens our understanding of the intricate molecular interactions involved. From this perspective, it is
481 plausible to suggest that *in vivo*, the dsRNA structures involving the inverted *Alu* elements in the Mut allele
482 might result from a network of interactions, potentially involving *Alu*1 and *Alu*_Ins, *Alu*2 and *Alu*_Ins, and even
483 complex combinations of segments from *Alu*1, *Alu*2, and *Alu*_Ins.
484 The formation of extensive dsRNA structures between inverted *Alu* elements is anticipated to occur at the
485 pre-mRNA level, hindering the normal splicing process of the *SPINK1* gene. Based upon current knowledge, this
486 splicing issue should often result in the pre-mRNA, which contains dsRNA, not being processed into mature
487 mRNA with a polyA tail, leading to its retention within the nucleus. Furthermore, even when dsRNA-containing
488 mRNA is fully processed, it may still often be retained within the nucleus instead of being transported to the
489 cytoplasm, as indicated by findings from a previous study [44]. With this context in mind, the aberrant RT-PCR
490 bands observed in the FLGEA assays should be seen as being indicative of dsRNA-containing, fully processed,
491 and aberrantly spliced mRNAs that have managed to be exported from the nucleus. Herein, we would like to
492 emphasize that these aberrant RT-PCR bands represent genuine products under our experimental conditions,
493 confirmed by the correct splicing out of introns 1 and 2 of the *SPINK1* gene. From the sequencing of these
494 aberrant bands, we inferred that intron 3 of the *SPINK1* gene was retained in these mRNA sequences. However,
495 within the constraints of our experimental setup, we were unable to capture the full-length transcripts that
496 retained intron 3. Instead, what we detected were 'template switching' events that are characteristic of
497 interactions involving the inverted *Alu* elements. Performing the reverse transcription at a higher temperature and
498 using a higher quality reverse transcriptase could potentially enable the detection of full-length, aberrantly
499 spliced transcripts.
500 Our study emphasizes the significance of utilizing appropriate model systems for functional analysis.
501 Without the FLGEA assay, the detailed mechanisms behind the pathogenic effects of the *Alu* insertion (*Alu*_Ins)

could not have been accurately identified. Indeed, informed by the current literature, one could logically infer a detrimental impact of *Alu*_Ins on the formation of the mRNA 3' end and on various post-transcriptional events, as demonstrated by the 3'-UTR reporter assay.

5. Conclusions

While it has been well-documented that secondary structures can influence splicing and that inverted *Alu* elements are capable of forming such structures, our research marks the first instance of demonstrating an *Alu* insertion variant causing human genetic disease by creating extensive dsRNA structures with pre-existing *Alu* elements. Considering the widespread presence of *Alu* elements in the human genome and the potential for new *Alu* insertions at almost any locus, our findings carry significant implications for detecting and interpreting the impact of *Alu* element insertion events in genes associated with human disease. This suggests that the analysis of potential *Alu* insertions should extend beyond coding regions and proximal intronic sequences to include deep intronic and non-coding regions as well. Furthermore, the functional impact of *Alu* insertions needs to be assessed in terms of their distances from, and orientations relative to, existing *Alu* elements within the affected genes.

Acknowledgments

We dedicate this work to the late Brice Felden, former Director of Inserm U1230 BRM (Bacterial RNAs and Medicine) at the Université de Rennes, Rennes, France. He provided expert insights into the formation of RNA secondary structures and their potential impact on gene expression regulation. Although sadly he was unable to see the project through to its completion, his influence was gratefully received and deeply felt.

Funding

This study was supported by the Institut National de la Santé et de la Recherche Médicale (INSERM), the Association des Pancréatites Chroniques Héréditaires (https://www.association-apch.org/), and the Association Gaétan Saleün (https://laboratoire-recherche-brest.net/), France. The funding bodies did not play any role in the study design, collection, analysis and interpretation of data or the writing of the article and the decision to submit it for publication.

Author contributions

Conceptualization, E.M., C.F. and J.M.C.; study design, E.M. and J.M.C.; methodology, E.M., S.M., B.V. and J.M.C.; experiments, E.M., S.M., B.V.; data interpretation, E.M., S.M., B.V., D.N.C., C.F. and J.M.C.; writing—original draft preparation, J.M.C.; writing—review and editing, E.M., S.M., B.V., D.N.C., C.F. and J.M.C.; project administration, J.M.C.; funding acquisition, C.F. and J.M.C. All authors have read and approved the final version of the manuscript and agree to be accountable for all aspects of the work, ensuring that questions related to the accuracy or integrity of any part of the work are appropriately investigated and resolved.

Data availability

All supporting data for this study are available within the article and its supplementary material.

Conflicts of interest

The authors are unaware of any conflicts of interest.

References

1. Lander ES, Linton LM, Birren B, Nusbaum C, Zody MC, Baldwin J, Devon K, Dewar K, Doyle M, FitzHugh W, et al: Initial sequencing and analysis of the human genome. *Nature* 2001, 409:860-921.
2. Kazazian HH, Jr., Moran JV: Mobile DNA in health and disease. *N Engl J Med* 2017, 377:361-370.
3. Feusier J, Watkins WS, Thomas J, Farrell A, Witherspoon DJ, Baird L, Ha H, Xing J, Jorde LB: Pedigree-based estimation of human mobile element retrotransposition rates. *Genome Res* 2019, 29:1567-1577.
4. Chen JM, Stenson PD, Cooper DN, Férec C: A systematic analysis of LINE-1 endonuclease-dependent retrotranspositional events causing human genetic disease. *Hum Genet* 2005, 117:411-427.
5. Hancks DC, Kazazian HH, Jr.: Roles for retrotransposon insertions in human disease. *Mob DNA* 2016, 7:9.
6. Chenais B: Transposable elements and human diseases: mechanisms and implication in the response to environmental pollutants. *Int J Mol Sci* 2022, 23.
7. Chen JM, Férec C, Cooper DN: LINE-1 endonuclease-dependent retrotranspositional events causing human genetic disease: mutation detection bias and multiple mechanisms of target gene disruption. *J Biomed Biotechnol* 2006, 2006:56182.
8. Venet T, Masson E, Talbotec C, Billiemaz K, Touraine R, Gay C, Destombe S, Cooper DN, Patural H, Chen JM, Férec C: Severe infantile isolated exocrine pancreatic insufficiency caused by the complete functional loss of the *SPINK1* gene. *Hum Mutat* 2017, 38:1660-1665.
9. Pinto A, Cunha C, Chaves R, Butchbach MER, Adega F: Comprehensive in silico analysis of retrotransposon insertions within the survival motor neuron genes involved in spinal muscular atrophy. *Biology (Basel)* 2022, 11.
10. Chemparathy A, Guen YL, Zeng Y, Gorzynski J, Jensen T, Yang C, Kasireddy N, Talozzi L, Belloy ME, Stewart I, et al: A 3'UTR insertion is a candidate causal variant at the *TMEM106B* locus associated with increased risk for FTLD-TDP. *medRxiv* 2023.
11. Ohmuraya M, Hirota M, Araki M, Mizushima N, Matsui M, Mizumoto T, Haruna K, Kume S, Takeya M, Ogawa M, et al: Autophagic cell death of pancreatic acinar cells in serine protease inhibitor Kazal type 3-deficient mice. *Gastroenterology* 2005, 129:696-705.
12. Kume K, Masamune A, Kikuta K, Shimosegawa T: [-215G>A; IVS3+2T>C] mutation in the *SPINK1* gene causes exon 3 skipping and loss of the trypsin binding site. *Gut* 2006, 55:1214.
13. Zou WB, Boulling A, Masson E, Cooper DN, Liao Z, Li ZS, Férec C, Chen JM: Clarifying the clinical relevance of *SPINK1* intronic variants in chronic pancreatitis. *Gut* 2016, 65:884-886.
14. Chen JM, Lin JH, Masson E, Liao Z, Férec C, Cooper DN, Hayden M: The experimentally obtained functional impact assessments of 5' splice site GT>GC variants differ markedly from those predicted. *Curr Genomics* 2020, 21:56-66.
15. Wu H, Lin JH, Tang XY, Marenne G, Zou WB, Schutz S, Masson E, Génin E, Fichou Y, Le Gac G, et al: Combining full-length gene assay and SpliceAI to interpret the splicing impact of all possible *SPINK1* coding variants. *Hum Genomics* 2024, 18:21.
16. Yamamoto T, Nakamura Y, Nishide J, Emi M, Ogawa M, Mori T, Matsubara K: Molecular cloning and nucleotide sequence of human pancreatic secretory trypsin inhibitor (*PSTI*) cDNA. *Biochem Biophys Res Commun* 1985, 132:605-612.
17. Horii A, Kobayashi T, Tomita N, Yamamoto T, Fukushige S, Murotsu T, Ogawa M, Mori T, Matsubara K: Primary structure of human pancreatic secretory trypsin inhibitor (*PSTI*) gene. *Biochem Biophys Res Commun* 1987, 149:635-641.
18. den Dunnen JT, Dalgleish R, Maglott DR, Hart RK, Greenblatt MS, McGowan-Jordan J, Roux AF, Smith T, Antonarakis SE, Taschner PE: HGVS recommendations for the description of sequence variants: 2016 update. *Hum Mutat* 2016, 37:564-569.
19. Boulling A, Le Gac G, Dujardin G, Chen JM, Férec C: The c.1275A>G putative chronic pancreatitis-associated synonymous polymorphism in the glycoprotein 2 (*GP2*) gene decreases exon 9 inclusion. *Mol Genet Metab* 2010, 99:319-324.

592 20. Boulling A, Witt H, Chandak GR, Masson E, Paliwal S, Bhaskar S, Reddy DN, Cooper DN, Chen JM, Férec
593 C: Assessing the pathological relevance of *SPINK1* promoter variants. *Eur J Hum Genet* 2011, 19:1066-
594 1073.
595 21. Zou WB, Boulling A, Masamune A, Issarapu P, Masson E, Wu H, Sun XT, Hu LH, Zhou DZ, He L, et al: No
596 association between *CEL-HYB* hybrid allele and chronic pancreatitis in Asian populations. *Gastroenterology*
597 2016, 150:1558-1560 e1555.
598 22. Gruber AR, Lorenz R, Bernhart SH, Neubock R, Hofacker IL: The Vienna RNA websuite. *Nucleic Acids Res*
599 2008, 36:W70-74.
600 23. Chen JM, Férec C, Cooper DN: A systematic analysis of disease-associated variants in the 3' regulatory
601 regions of human protein-coding genes I: general principles and overview. *Hum Genet* 2006, 120:1-21.
602 24. Steri M, Idda ML, Whalen MB, Orru V: Genetic variants in mRNA untranslated regions. *Wiley Interdiscip*
603 *Rev RNA* 2018, 9:e1474.
604 25. Griesemer D, Xue JR, Reilly SK, Ulirsch JC, Kukreja K, Davis JR, Kanai M, Yang DK, Butts JC, Guney
605 MH, et al: Genome-wide functional screen of 3'UTR variants uncovers causal variants for human disease and
606 evolution. *Cell* 2021, 184:5247-5260 e5219.
607 26. Romo L, Findlay SD, Burge CB: Regulatory features aid interpretation of 3'UTR variants. *Am J Hum Genet*
608 2024, 111:350-363.
609 27. Drexler HL, Choquet K, Churchman LS: Splicing kinetics and coordination revealed by direct nascent RNA
610 sequencing through nanopores. *Mol Cell* 2020, 77:985-998 e988.
611 28. Gehring NH, Roignant JY: Anything but ordinary - emerging splicing mechanisms in eukaryotic gene
612 regulation. *Trends Genet* 2021, 37:355-372.
613 29. Rogalska ME, Vivori C, Valcarcel J: Regulation of pre-mRNA splicing: roles in physiology and disease, and
614 therapeutic prospects. *Nat Rev Genet* 2023, 24:251-269.
615 30. Solnick D: Alternative splicing caused by RNA secondary structure. *Cell* 1985, 43:667-676.
616 31. Clouet d'Orval B, d'Aubenton Carafa Y, Sirand-Pugnet P, Gallego M, Brody E, Marie J: RNA secondary
617 structure repression of a muscle-specific exon in HeLa cell nuclear extracts. *Science* 1991, 252:1823-1828.
618 32. Buratti E, Baralle FE: Influence of RNA secondary structure on the pre-mRNA splicing process. *Mol Cell*
619 *Biol* 2004, 24:10505-10514.
620 33. Chen JM, Férec C, Cooper DN: A systematic analysis of disease-associated variants in the 3' regulatory
621 regions of human protein-coding genes II: the importance of mRNA secondary structure in assessing the
622 functionality of 3' UTR variants. *Hum Genet* 2006, 120:301-333.
623 34. Daniel C, Silberberg G, Behm M, Ohman M: Alu elements shape the primate transcriptome by cis-regulation
624 of RNA editing. *Genome Biol* 2014, 15:R28.
625 35. Bazak L, Levanon EY, Eisenberg E: Genome-wide analysis of *Alu* editability. *Nucleic Acids Res* 2014,
626 42:6876-6884.
627 36. Ku J, Lee K, Ku D, Kim S, Lee J, Bang H, Kim N, Do H, Lee H, Lim C, et al: Alternative polyadenylation
628 determines the functional landscape of inverted *Alu* repeats. *Mol Cell* 2024.
629 37. Lev-Maor G, Ram O, Kim E, Sela N, Goren A, Levanon EY, Ast G: Intronic *Alu*s influence alternative
630 splicing. *PLoS Genet* 2008, 4:e1000204.
631 38. Kristensen LS, Andersen MS, Stagsted LVW, Ebbesen KK, Hansen TB, Kjems J: The biogenesis, biology
632 and characterization of circular RNAs. *Nat Rev Genet* 2019, 20:675-691.
633 39. Welden JR, Stamm S: Pre-mRNA structures forming circular RNAs. *Biochim Biophys Acta Gene Regul*
634 *Mech* 2019:194410.
635 40. Jeck WR, Sorrentino JA, Wang K, Slevin MK, Burd CE, Liu J, Marzluff WF, Sharpless NE: Circular RNAs
636 are abundant, conserved, and associated with *ALU* repeats. *RNA* 2013, 19:141-157.
637 41. Liang D, Wilusz JE: Short intronic repeat sequences facilitate circular RNA production. *Genes Dev* 2014,
638 28:2233-2247.
639 42. Zhang XO, Wang HB, Zhang Y, Lu X, Chen LL, Yang L: Complementary sequence-mediated exon
640 circularization. *Cell* 2014, 159:134-147.
641 43. Cocquet J, Chong A, Zhang G, Veitia RA: Reverse transcriptase template switching and false alternative
642 transcripts. *Genomics* 2006, 88:127-131.
643 44. Chen LL, DeCerbo JN, Carmichael GG: *Alu* element-mediated gene silencing. *EMBO J* 2008, 27:1694-1705.